Chapter 2
Principle and Design

As discussed in Chapter 1, the MEMS optical pickup head is composed of several chips bonded together, as shown in Figure 2-1. The top wafer is like a cap to cover the optical bench and to hold the lens actuator. The middle wafer is a spacer wafer to make room for the popped up optical components. It can also fix the fiber using V-grooves, too. The bottom wafer is the optical bench. Figure 2-1 (b) also shows the side view of the devices. To facilitate the alignment between chips during bonding, bulk micromachined structures can be fabricated on the surfaces of the chips, as shown in Figure 2-1 (c).

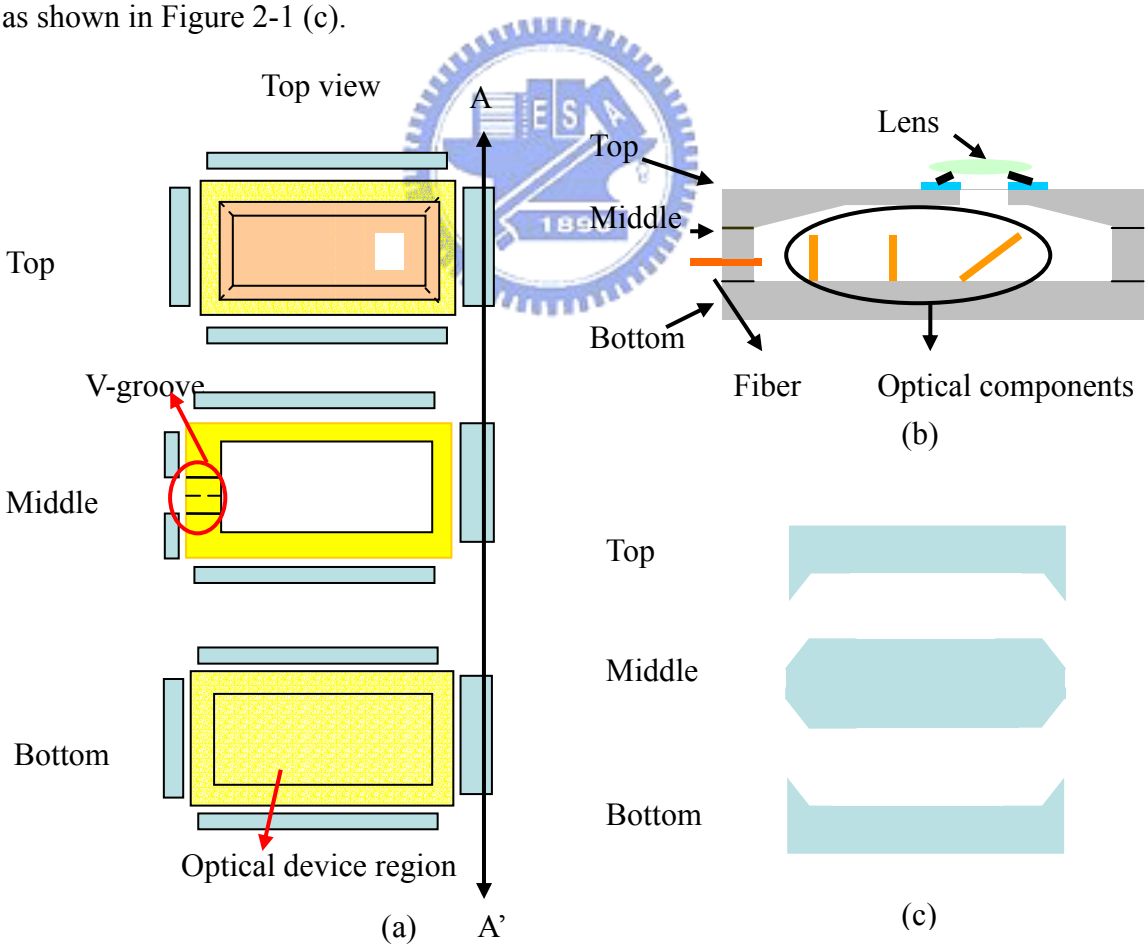

Figure 2-1: Proposed MEMS pickup (a) top view (b) side view (c) AA' cross section.

In the first part, the basic principle of self-alignment structures by wet etching is discussed. In the second part, a novel MOEMS structure employing SOI wafers and SU-8 photoresist as structure materials is proposed.

2-1 Self alignment structure in silicon

Wet anisotropic chemical etching has been developed for the fabrication of passive alignment structures in silicon [5] [6]. The simplest and most widely used micromachined structure is the V-grooves on (100) silicon wafers. The grooves are defined by (111) planes that are slanted at 54.7° to the substrate as shown in Figure 2-2. The V-groove structures have been used to fix the position of optical fibers or to monitor the etching depth [5] [6]. Most of the reported anisotropic etchants are aqueous alkaline solutions, either organic or inorganic. Among them the most widely used is potassium hydroxide (KOH). The anisotropy is strongly dependent on the etchant composition, etchant concentration, dopant concentration, temperature and even stirring. The smoothness of the etched surface can be improved by adding IPA to pure KOH solution [6]. For KOH, the ratio of etch rates for the three major crystallographic planes is approximately (111): (110): (100) = 1:400:600. As a consequence, the KOH etching of (100) silicon results in the dissolution of the nearest (110) and (100) planes whereas the (111) planes act as the boundary walls that defines the final shape of the etched pit.

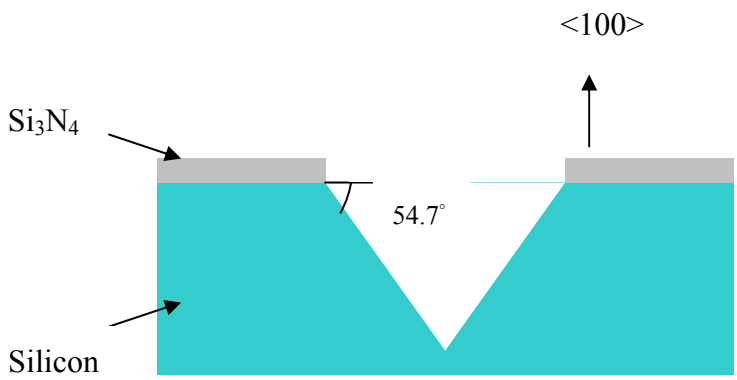

Figure 2-2 V-groove in (100) silicon substrate.

2-1-1 Self alignment structure design

Figure 2-3 shows the alignment structures on two of the wafers in the MEMS pickup. In Figure 2-3(a), there are four rectangular and four square groove structures around the optical bench area on the bottom wafer. In Figure 2-3(b) the top wafer has four ridge structures. Since it is more difficult to control the etching depth than the line width of the pattern, the alignment mechanism is based on the pattern width of the ridge and corresponding groove structures. As shown in Figure 2-3 (a), W1 is the line width of ridge structures and W2 is the bottom width of groove structures. If W1<W2, there will be a gap in the lateral orientation, as shown in Figure 2-4 (b). So it can not be used as a precise alignment mechanism. If $W1 \geq W2$, as shown in Figures 2-4 (c), (d), there is no misalignment in the horizontal direction. However, Figure 2-4 (c) is not easy to achieve because it has many variations in wet etching methods. Therefore, structures with $W1 \geq W2$ were adopted. Table 2-1 summarizes the dimensions of the self alignment structures, including the width and length, and depth of ridge and groove structures.

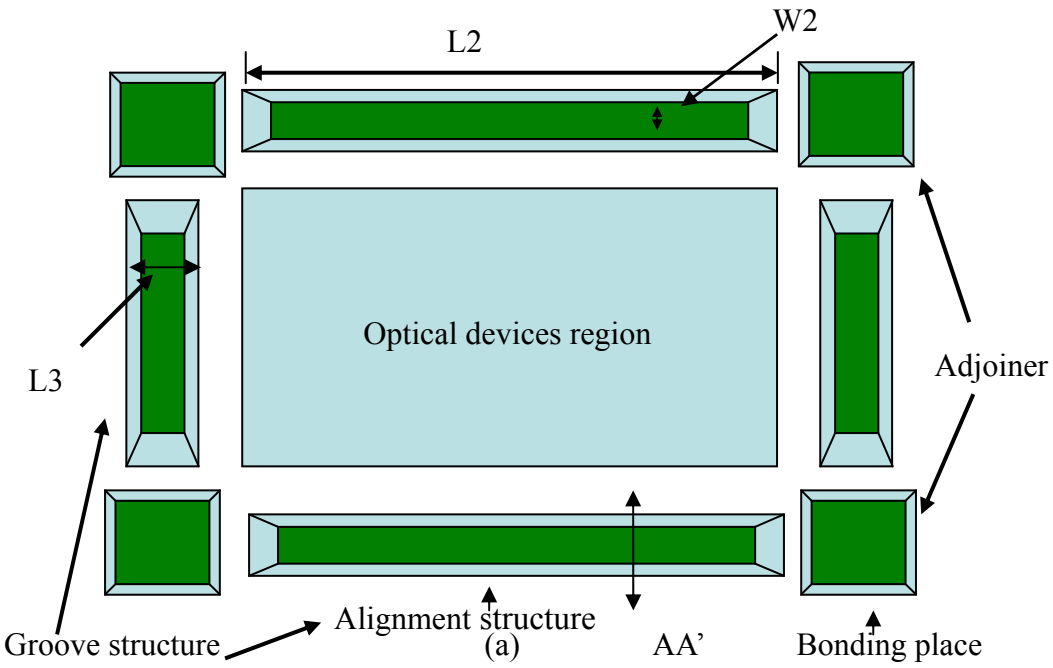

Figure2-3: Self -alignment structures (a) top view of the bottom wafer (b) top view of top wafer.

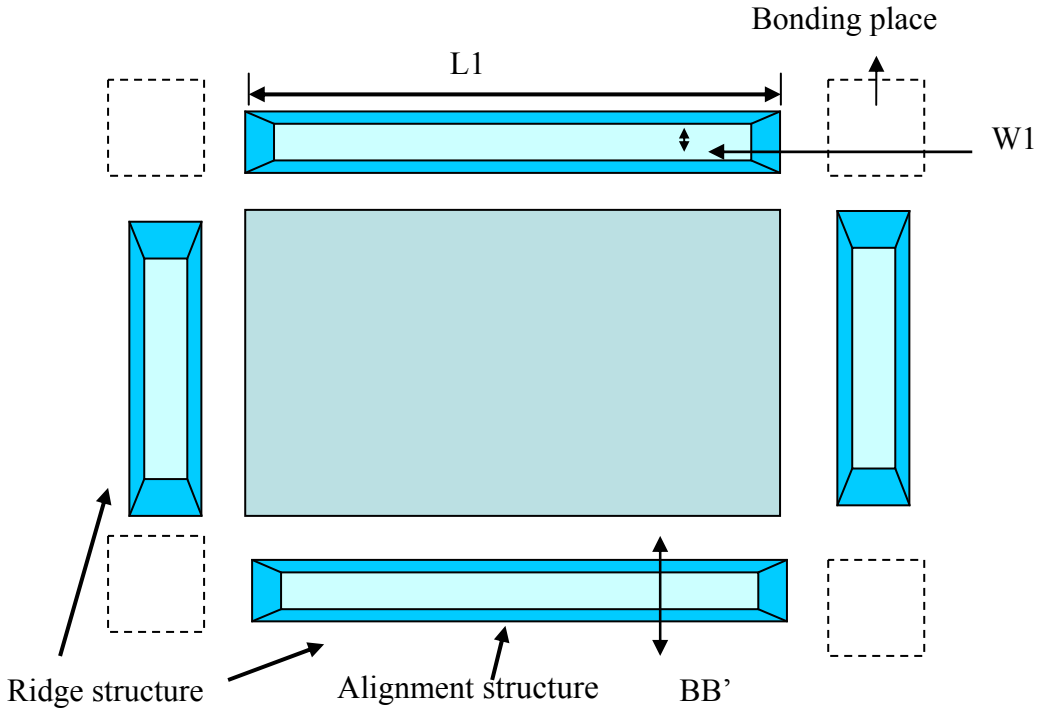

Figure2-3: Self -alignment structures (a) top view of the bottom wafer (b) top view of top wafer. (Continued)

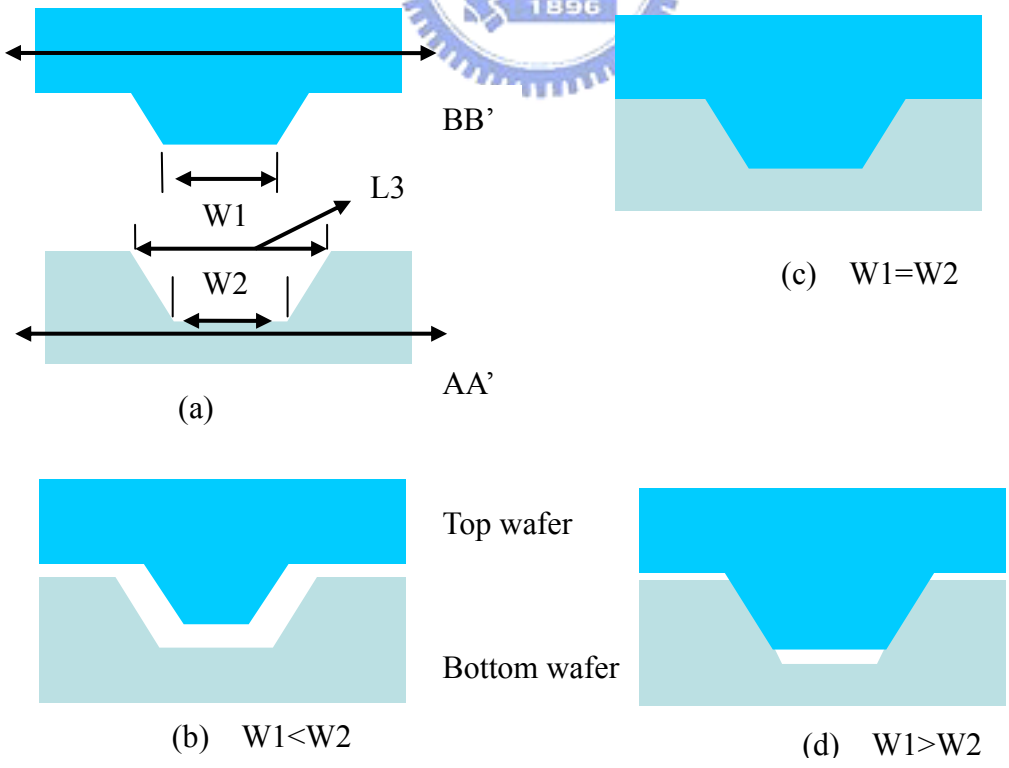

Figure 2-4 Cross section view of the segment AA’, BB’.

Table 2-1: Dimensions of the self alignment structure.

Depth of groove	Line width of ridge structure (W1)	Length of ridge structure (L1)	Bottom width of groove Structure (W2)	Line width of groove structure (L3)	Length of groove Structure (L2)
50um	25um	5070um	24.2um	95um	5000um
	50um	5070um	49.2um	120um	5000um
	75um	5070um	74.2um	145um	5000um
75um	25um	5106um	24.8um	131um	5000um
	50um	5106um	49.8um	156um	5000um
	75um	5106um	74.8um	181um	5000um
100um	25um	5141um	24.4um	166um	5000um
	50um	5141um	49.4um	191um	5000um
	75um	5141um	74.4um	216um	5000um
150um	50um	5212um	49.6um	262um	5000um
	75um	5212um	74.6um	287um	5000um
	100um	5212um	99.6um	312um	5000um

2-2 Stress beam using SU-8 and SOI wafer

In this thesis, SU-8 is used for the stress-induced beam and the anchor of the flipped-up micromirror. In addition, SU-8 also can be used for optical components for its transparency in visible spectrum. SOI wafers are adopted because it can simplify the process, improve the flatness of micromirrors and easily be integrated with surface micromachining.

2-2-1 Properties of SU-8

SU-8 is a negative-imaging epoxy-type near-UV photoresist consisting of multifunctional highly branched polymeric epoxy resin (EPON SU-8). A single molecule of SU-8 typically contains 8 epoxy groups (hence the 8 in SU-8) in a bisphenol A novolac glycidyl ether as shown in Figure 2-5. The specific properties of SU-8 enable ultra-thick layers of high uniformity with low edge bead and smooth surface up to 500mm by a single coating step. Near UV exposure with low doses which yields patterns with nearly vertical sidewalls and aspect ratio >15.

SU-8 is most commonly processed with conventional near UV (350-400nm) radiation, in which i-line (365nm) is recommended. A normal process is spin, coat, soft bake, expose, post expose bake (PEB) followed by develop. A controlled hard bake is recommended to further cross-link the imaged SU-8 2000 structures when they will remain as part of the device. A baseline process is shown in Figure 2-6.

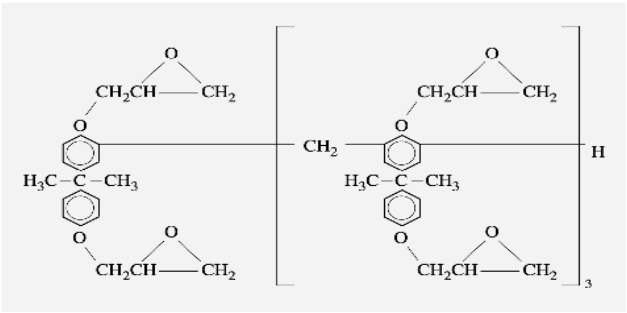

Formula VI

Glycidyl ether of bisphenol A—SU-8.

Figure 2-5 Structure of SU-8 [25].

.

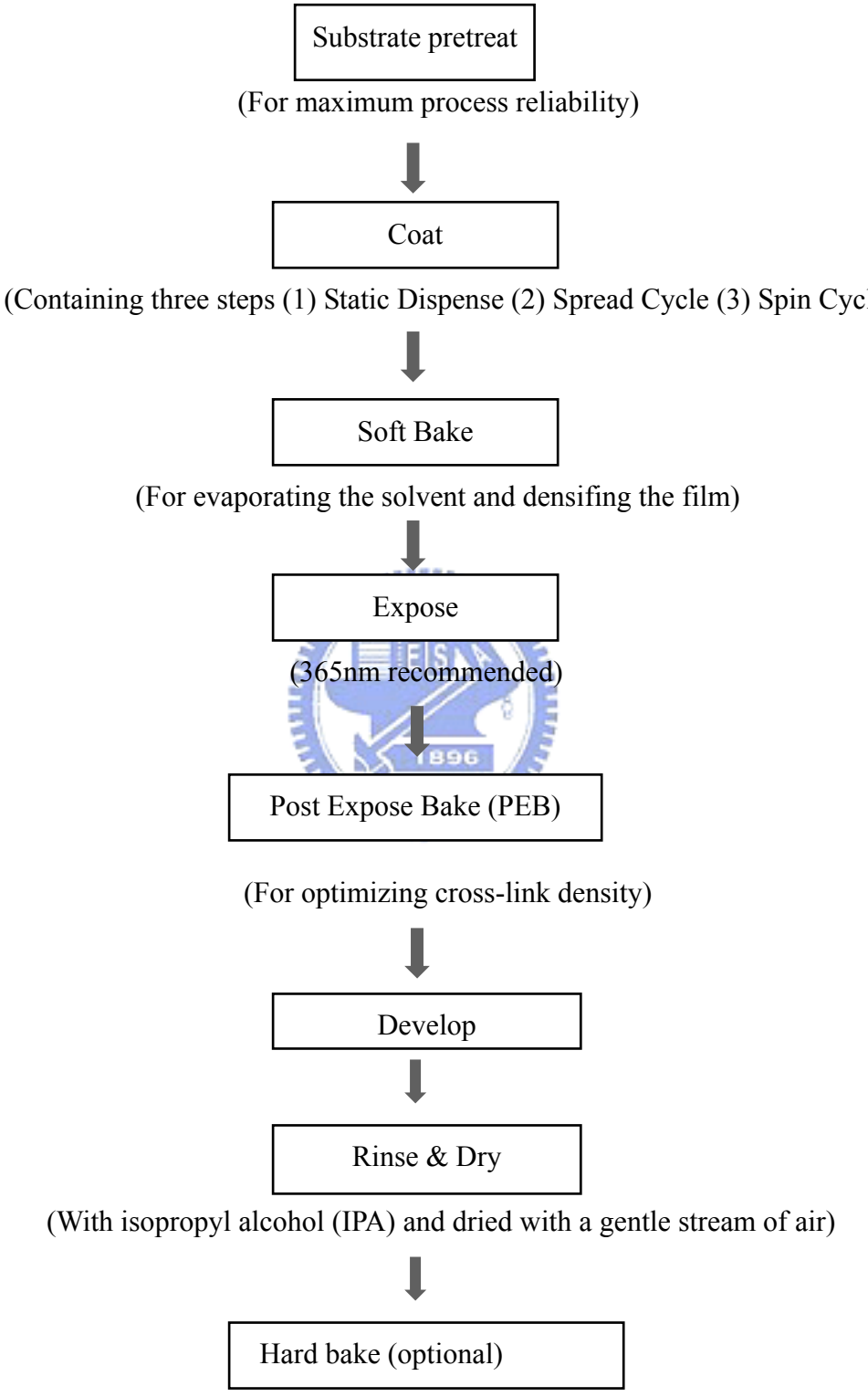

Figure 2-6: A baseline process of SU-8.

2-2-2 Stress of SU-8

Substrate/wafer stress due to thick resist coatings is a key issue for many applications. After prebake, a small tensile stress is introduced by the difference between the thermal expansion coefficients (TECs) of the wafer and SU-8 [26]. The stress is small because during the cooling phase of the prebake, polymer chain rearrangements take place in the resists that are not crosslinked. The main stress is generated as the crosslinked SU-8 cools down especially after hardbaking. In addition to the thermo-mechanical stress introduced by the difference of the TECs, stress due to resist polymerization is also present.

For resist thicknesses comparable to the wafer thickness, this stress can be high and consequently the wafer is bowed. Table 2-2 shows the measured bowing of a silicon wafer coated with SU-8. In this experiment, four 520-um-thick silicon wafers were used. SU-8 photoresist was spin coated on the silicon wafers and its thickness was 21um. The four silicon wafers were hardbaked for 0 min, 10 min, 20 min and 30min, respectively. Before hardbake, the warp of silicon is small. However, after hardbake the warp of silicon is large because of the tensile stress of SU-8. The calculated residual stress of SU-8, using Young's Modulus = 4.6GPa, [27] is also shown in Table 2-1. The obtained value after hard bake is chose to these reported in literature [26].

72mm

SU-8
Si (520um)

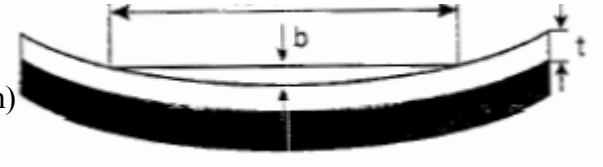

Table 2-2: Wafer bowing due to the stress in the SU-8 layer. The bowing was measured over a 72mm distance of a fully exposed 4inch, 520um thick silicon wafer.

	Hardbake	Before hardbake	After hardbake	Difference	Stress of SU-8
Sample1	0min	b=7.7um	b=28.6um	20.9um	13Mpa
Sample2	10min	b=16.1um	b=55.1um	39um	24Mpa
Sample3	20min	b=-1.9um	b=41.5um	43.4um	27Mpa
Sample4	30min	b=-4.2um	b=39.2um	43.4um	27Mpa

2-2-3 Residual stress beam

Residual stress is a tension or compression stress which exists in the bulk of a material without the application of an external load (applied force, displacement or thermal gradient). Residual stress is produced by heterogeneous plastic deformation, thermal contraction or phase transformation induced by manufacturing processes. It can also be divided into thermal stress and intrinsic stress according to its source. The formula of the thermal stress is given by $\sigma_{th} = E\Delta\alpha\Delta T$, where E is the Young's modulus, $\Delta\alpha$ is the difference in the coefficients of thermal expansion between the

film and the substrate and ΔT is the difference between the deposition temperature and the room temperature. If the temperature of fabrication is high, the main stress is produced by thermal stress. The intrinsic stress, σ_i, reflects the internal structure of a material and is less clearly understood than the thermal stress. Several phenomena may contribute to σ_i, making its analysis very complex. Intrinsic stress depends on thickness, deposition rate (locking in defects), deposition temperature, ambient pressure, method of film preparation, type of substrate (lattice mismatch), incorporation of impurities during growth, etc.

Residual stress can be tensile or compressive. In a bimorph beam, the upper layer that has a tensile stress and the lower layer that has zero stress make the cantilever beam to curve upwards, as shown in Figure 2-7(a). If the upper layer has a compressive stress and the lower layer has zero stress, the cantilever beam bows downwards, as shown in Figure 2-7(b). Excessive compressive or tensile stress results in splintering, cracking and adhesion problems of the film to the substrate. Here the drawback is transferred to an advantage to apply a force to pop up other micro structures. In this thesis, the residual stress beams are used to lift up the reflective micromirror. The analysis of the stress-induced beam is discussed in the next sections.

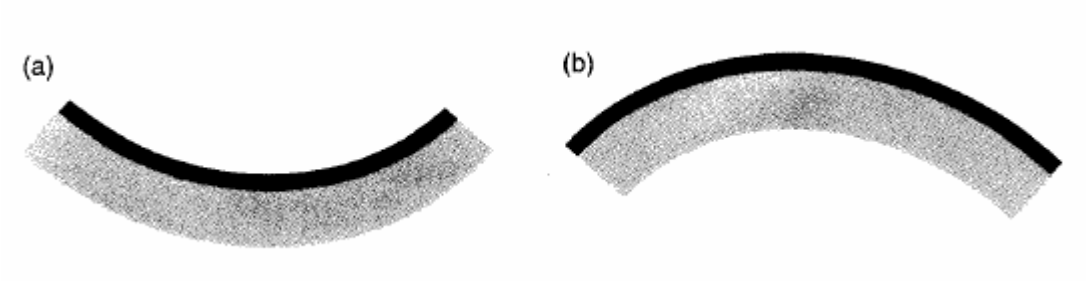

Figure 2-7: Two types of stress in the upper layer, (a) tensile stress (b) compressive stress.

2-2-4 Stress beam design

The composite beam shown schematically in Figure 2-8 is a micro cantilever beam composed of two materials with different residual stresses, σ_1 and σ_2, as well as different Young's modulus, E_1 and E_2 [28].

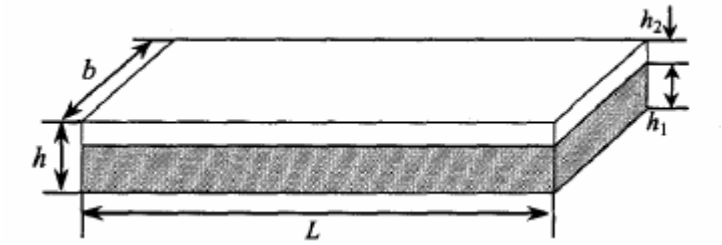

Figure 2-8: Dimensions of a cantilever beam.

Assuming the resultant forces, P_1 and P_2, act at the center of their respective cross sections, the force and moment balance can be made, as shown in Figure 2-9 [29]:

$$P_1 = P_2 = P$$

$$P \cdot \frac{h}{2} = M_1 + M_2 = M \quad , \tag{2-1}$$

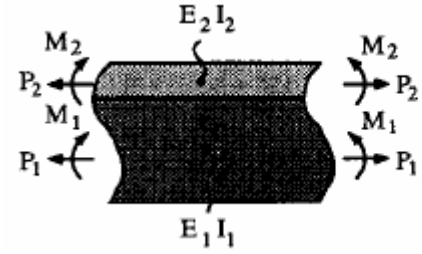

Figure 2-9 Resulting forces and moments.

where h_1 and h_2 are the thickness of the lower film and the upper film, respectively and $h=h_1+h_2$ is the total thickness of the beam. To calculate the moment-curvature relations for each material, an equivalent beam strength $(EI)_{equiv}$ can be defined [30, 31]

$$(E \cdot I)_{equiv} = \frac{E_2 \cdot b \cdot h_2^3}{12(1 + m \cdot n)} \cdot K \ , \tag{2-2}$$

where $$K=1+4mn+6mn^2+4mn^3+m^2n^4 \tag{2-3}$$

$$m = \frac{E_1}{E_2} \quad \text{and} \quad n = \frac{h_1}{h_2} \tag{2-4}$$

and E_1 and E_2 are the Young's modulus of the lower film and the upper film, respectively. The relationship between the stress-induced internal force (P) and the radius of curvature (ρ) can be determined:

$$P = \frac{2 \cdot (E \cdot I)_{equiv}}{h \cdot \rho} \tag{2-5}$$

The radius of curvature (ρ) is constant along the beam, since the internal force (P) and the beam geometry do not vary.

An additional condition is that of zero slip at the interface. The strain in each film is composed of three components: one due to the residual stresses σ_1 and σ_2, one due to the axial force P, and one due to the curvature ρ of the beam. Setting the sum of the three components in one material equal to that of the other at the interface is that:

$$\frac{\sigma_1}{E_1} + \frac{p}{E_1 h_1 b} + \frac{h_1}{2\rho} = \frac{\sigma_2}{E_2} - \frac{P}{E_2 h_2 b} - \frac{h_2}{2\rho} \tag{2-6}$$

The radius of curvature of the pre-biased flexure is obtained by solving Eqs. (2-2), (2-5) and (2-6),

$$\frac{1}{\rho} = \frac{6(m \cdot \sigma_2 - \sigma_1)}{h \cdot E_2 (3m + K[n(1+n)^2]^{-1})} \tag{2-7}$$

With the radius of curvature known, the end deflection of the beam can be calculated from trigonometry. The deflection perpendicular to the unreleased position for a given beam length, L, with radius of curvature ρ is given by

$$\delta = \rho(1 - \cos(L / \rho)) \qquad (2\text{-}8)$$

- **Simulation**

The bending height of the bimorph residual stress beam is calculated by utilizing the above theory and simulated by IntelliSuite. The material and geometric parameter of a SU-8/single crystal silicon (SCS) bimorph are E_1 = 190GPa (SCS), E_2 = 4.6GPa (SU-8) [27], h_1 = 5μm, h_2 =15μm, σ_1 = 0MPa and σ_2 = 27MPa. The material and geometric parameter of a Gold/SCS bimorph are E_1 = 190GPa (SCS), E_2 = 78GPa (gold) [32], h_1 =5μm, h_2 = 0.5μm, σ_1 = 0MPa and σ_2 = 270MPa. The residual stresses of SU-8 and gold are obtained from Ref [33] and measurement results.

In this thesis, gold is used for metal lines and reflective surfaces. However, the stress of gold is large and gold induced stress beam is also possible in the process. Therefore, The deflections of a SU-8/SCS and a gold/SCS residual stress beams, calculated from Eqs. (2-4), (2-7), and a SU-8/SCS residual stress beam which simulated by IntelliSuite, are shown in Figure 2-10. Under the above process parameters, the deflection of SU-8/SCS is larger than gold/SCS. So, the SU-8 induced stress beam is adopted.

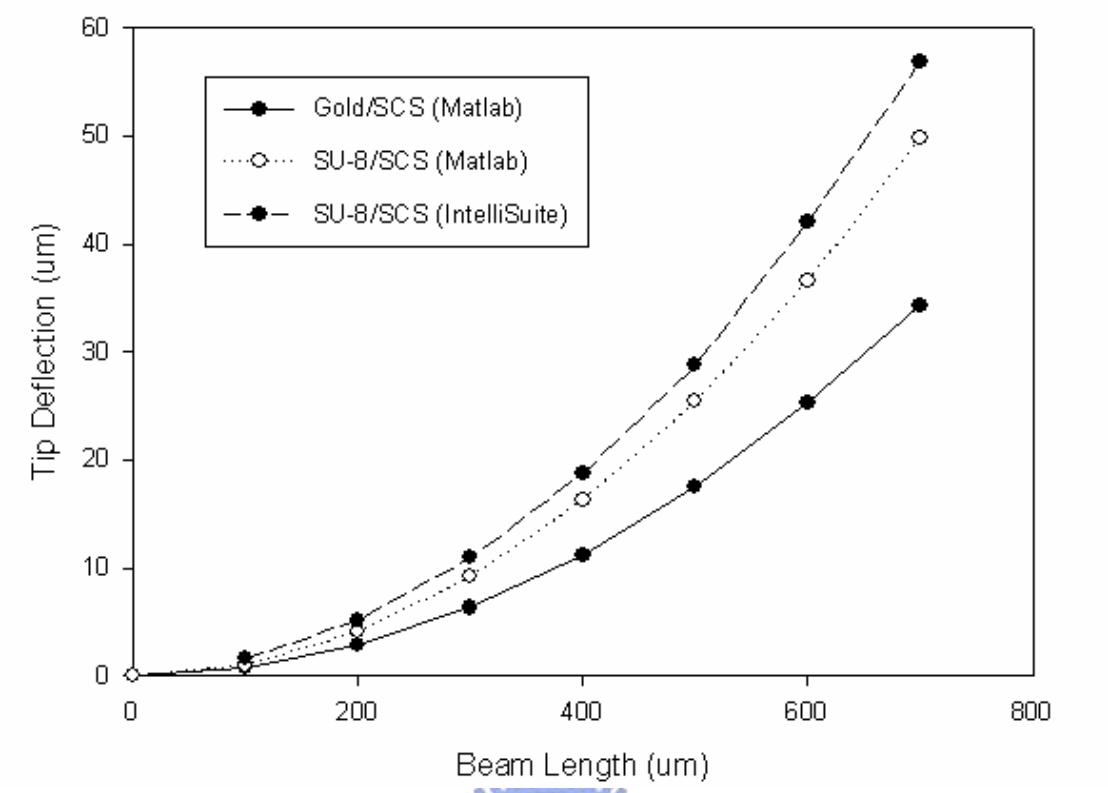

Figure 2-10: Deflection vs. beam length.

Figure 2-11 is the IntelliSuite simulation result of a SU-8/SCS bimorph as described above. The length and width of the beam are 460μm and 150μm, respectively. The simulation shows an end deflection of 23.25μm.

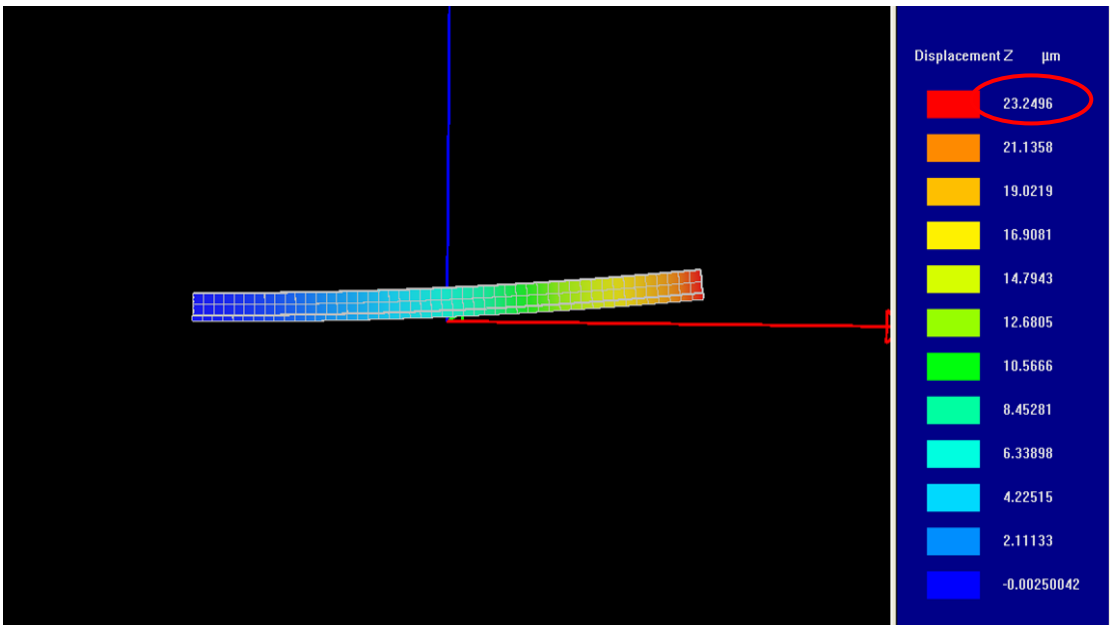

Figure 2-11: 3D plot of the IntelliSuite simulation result.

2-2-5 Integrated device design

In the past, poly silicon has been the most common material for microstructures. However, it may get curved after releasing due to stress. On the other hand, SOI wafers almost have no stress. Therefore, micromirror made by the top silicon layer of SOI wafers can have a better optical performance. One of the goals of the thesis is to fabricate a photodetector underneath a 135° micro mirror, as shown in Figure 1-3. As discussed in the previous sections, SOI wafer is chosen so that the photodetector can be easily integrated with a flat micro mirror. Figure 2-12 shows the layout of a 135° reflective micromirror integrated with photodiodes, which are used to detect the optical signals. In Figure 2-12, X is the middle stress beam, Y is the longest stress beam and Z is the shortest stress beam. Figure 2-13 is the A-A' cross section view in Figure 2-12. The height of the optical axis is 400 um and spot size is 600 um. Therefore, the length and width of the micromirror in Figure 2-12 are 1000 um and 700 um. The micromirror will be fixed at 135° by the latch beam, which is 400um in length, as shown in Figure 2-13. SU-8 induced stress beams are used to lift up the micromirror a little so that micro probes can be inserted more easily to assemble the final device. Table 2-3 shows the dimension of the SU-8 stress beam in Figure 2-12.

- **Summary**

A novel fabrication process is proposed to take advantage of the single crystalline nature of SOI substrates and the easiness of processing and optical transparency of SU-8. An integrated device with a 135° mirror, latching mechanism, stressed lifting arm, and photodiodes are demonstrated.

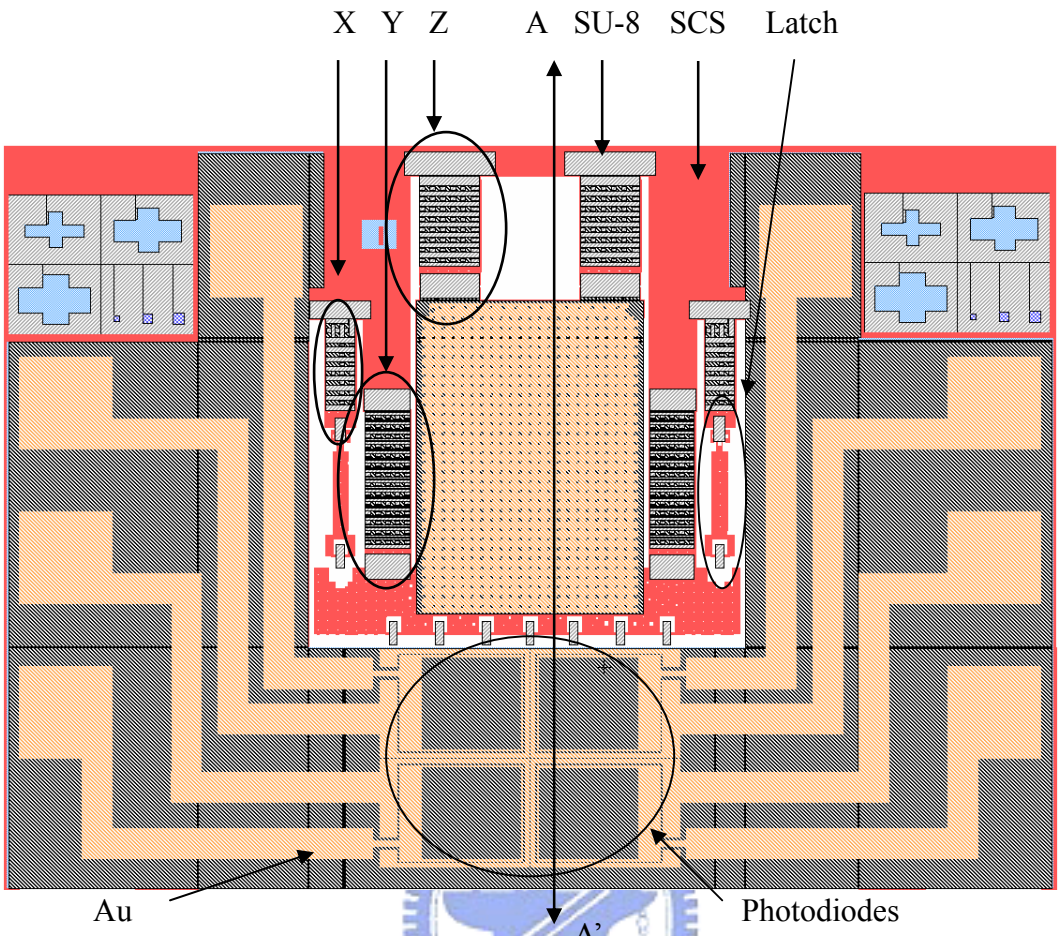

Figure 2-12: Layout of a 135° flipped mirror integrated with photo diodes.

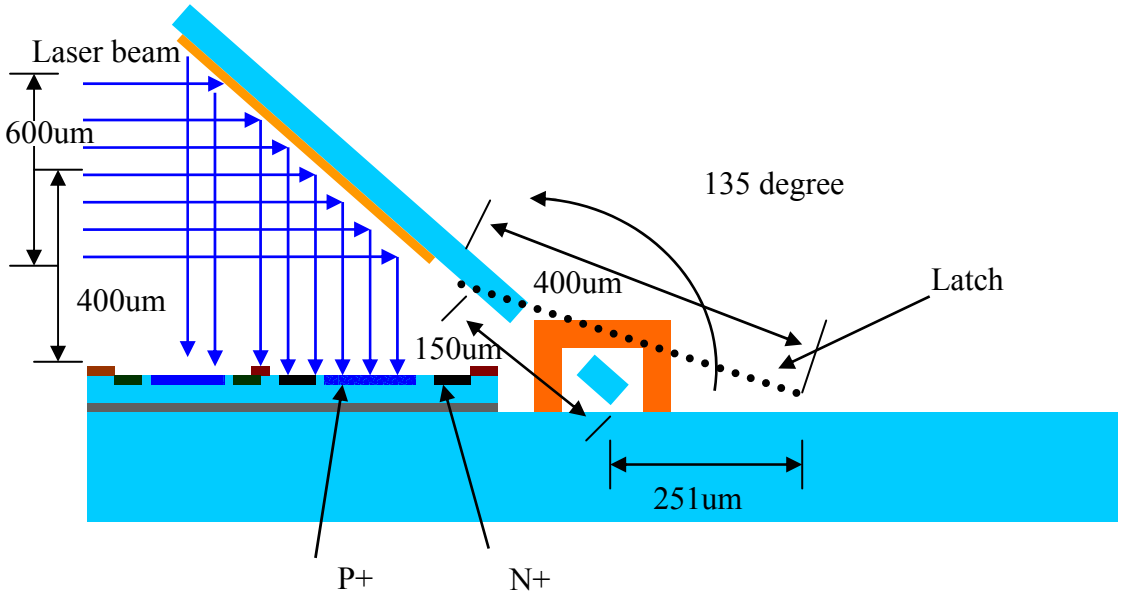

Figure 2-13: A-A' cross section view of the device in Figure 2-12 after assembly.

Table 2-3: Dimensions of the SU-8 stress beam.

Stress beam	Length(um)	Width(um)	Z displacement
X	300	100	10.87 um
Y	460	150	25.54 um
Z	290	200	10.15 um